JOURNAL OF GEOPHYSICAL RESEARCH: SPACE PHYSICS, VOL. 118, 724–731, doi:10.1002/jgra.50103, 2013

Comparative analysis of low-altitude ENA emissions in two substorms

N. Buzulukova,[1,2] M.-C. Fok,[1] E. Roelof,[3] J. Redfern,[4] J. Goldstein,[4,5] P. Valek,[4,5] and D. McComas[4,5]

Received 23 July 2012; revised 20 December 2012; accepted 22 December 2012; published 25 February 2013.

[1] We report on the dynamics of low-altitude energetic neutral atom (ENA) emissions during two substorms that occurred during the main phases of two storms: (1) a CIR-driven storm on 11 October 2008 and (2) a coronal mass ejection (CME)-driven storm on 5 April 2010. For both of these storms, we have complementary spacecraft and ground-based observations. The dual-spacecraft Two Wide-angle Imaging Neutral-atom Spectrometers (TWINS) mission obtained ENA images containing low-altitude emissions (LAEs). Substorm dynamics is inferred from THEMIS all-sky imagers. TWINS-observed LAEs are compared with trapped/loss cone proton fluxes from the low-altitude NOAA/MetOp spacecraft constellation. We find that the timing and intensity profiles of LAEs are different for the two selected events. For the 11 October 2008 event, the LAEs rise during substorm recovery phase and storm main phase. On 5 April 2010, the LAEs tend to peak near substorm onset. We argue that the different LAE behavior results from different pitch-angle distributions (PADs) of the ion source population. Ion PADs are isotropic during substorm recovery phase for the 11 October 2008 event and have empty loss cone for the 5 April 2010 event. For both cases, LAE intensification marks the onset of activity in the magnetotail and precedes the large substorm onset. We conclude that the LAE production starts in the transition region between the magnetotail and ring current and may expand/move into the inner magnetosphere together with ring current formation.

Citation: Buzulukova, N., M.-C. Fok, E. Roelof, J. Redfern, J. Goldstein, P. Valek, and D. McComas (2013), Comparative analysis of low-altitude ENA emissions in two substorms, *J. Geophys. Res. Space Physics*, *118*, 724–731, doi:10.1002/jgra.50103.

1. Introduction

[2] Energetic neutral atom (ENA) imaging is a very useful tool for studying ring current and plasma sheet dynamics during geomagnetic storms and substorms. Near-Earth ENA emissions can be divided into two types: (1) optically thin emissions originating from high altitudes (i.e., the ring current and/or plasma sheet) and (2) optically thick emissions generated at low altitudes observable near the Earth's limb. The high-altitude emissions (HAEs) are formed in single-collision interactions when magnetospheric plasma undergoes charge exchange with cold neutral hydrogen from the geocorona. In contrast, low-altitude emissions (LAEs) are the result of multiple charge-exchange and electron-stripping collisions involving dense exospheric neutrals (mainly atomic oxygen). The first images of LAEs were obtained by the Swedish ASTRID satellite [*Brandt et al*., 1997]. The IMAGE mission (2000–2005) obtained LAE images across a broad energy range (1–30 keV and 20–500 keV for the MENA and HENA instruments, respectively). *Pollock et al*. [2009] compared HENA-observed LAEs with NOAA-observed precipitating protons during the giant 2003 Halloween storm and concluded that the spatial structure of LAEs reflects that of precipitating protons. *Bazell et al*. [2010] demonstrated that LAEs observed by TWINS agreed with the ENAs that would be produced by ions simultaneously measured in situ by the DMSP spacecraft, both in spatial and energy dependence.

[3] Both LAEs and HAEs are sensitive to viewing geometry; LAEs more so because their origin is in particles mirroring near the Earth with local pitch angles close to 90°. This geometry favors LAE observations near the Earth limb from the opposite MLT sector, inside a narrow cone (tens of degrees) [*Pollock et al*., 2009; *Bazell et al*., 2010]. *Bazell et al*. [2010] introduced a thick target approximation (TTA) to estimate the LAE intensity. In the TTA approach, the peak intensity of LAE-associated ENAs escaping the multi-collisional region is proportional to the incident proton intensity near the same magnetic field line, within a factor of

[1]Geospace Physics Laboratory, NASA Goddard Space Flight Center, Greenbelt, Maryland, USA.
[2]Department of Astronomy, University of Maryland, College Park, Maryland, USA.
[3]Johns Hopkins University, Applied Physics Laboratory, Laurel, Maryland, USA.
[4]Southwest Research Institute, Texas, USA.
[5]University of Texas, San Antonio, Texas, USA.

Corresponding author: N. Buzulukova, M.-C. Fok, NASA Goddard Space Flight Center, Mail Code 673, 8800 Greenbelt Road Greenbelt, MD 20771, USA. (nbuzulukova@gmail.com)

2169-9380/13/10.1002/jgra.50103

~1–5. The TTA explains why LAEs are bright in comparison with HAEs from ring current.

[4] Using TWINS data from a moderate storm on 22 July 2009, *Valek et al.* [2010] compared the temporal evolutions of LAEs and HAEs and concluded that these two emissions had quite different intensity-versus-time profiles, most likely a manifestation of different controlling processes. The substorm response of these two emission types has not been compared. Although the response of HAEs to substorms is reported in several studies (*Pollock et al.* [2003] and references therein; [*Mende et al.*, 2002]), the LAE substorm response still requires quantification.

[5] In this report, we analyze the temporal evolution of LAEs observed by TWINS spectrometers [*McComas et al.*, 2009] during two substorms, each of which occurred at the main phase of two geomagnetic storms. From Dst-index response, both events can be characterized as moderate geomagnetic storms with $Dst_{min} \sim -60\,nT$. The other characteristics of the two events, however, were different.

[6] On 11 October 2008, a substorm occurred during the main phase of a corotating-interaction region (CIR)-driven storm. Ring current ENAs (i.e., HAEs) from this event were analyzed in *Buzulukova et al.* [2010]. The LAEs for ~10 UT were analyzed in *Bazell et al.* [2010]. The 5 April substorm occurred during a coronal mass ejection (CME)-driven storm featuring widespread auroral activity, as well as a failure of the Galaxy 15 telecommunications satellite [*Connors et al.*, 2011; *McComas et al.*, 2012]. For the intervals selected from these two events, the viewing geometry for LAEs was approximately the same, facilitating the direct comparison of observations of the nightside auroral oval.

[7] In this paper, TWINS-observed LAEs are compared with trapped/loss cone protons observed by the MEPED telescopes on the NOAA and MetOp satellites at ~800 km altitude. We find that the timing and intensity profiles of LAEs are different for the two events and explain the different LAE behavior as resulting from different pitch angle distributions of the ring current population. We also note that the LAE responses for our two events both precede large substorm onsets.

2. 11 October 2008 Event

[8] Figure 1 displays the LAE index (panel a), AU/AL/SYMH geomagnetic indices (panel b), and THEMIS all-sky imager observations for three stations (FSIM, YKNF, and FSMI; plates c–e) for the 11 October 2008 event, 0730–1030 UT. THEMIS images are auroral white-light keograms produced by vertical scans of individual auroral images at 6-s cadence (see *Mende et al.* [2008] for details).

[9] The LAE index for a given energy is defined as the intensity of the brightest pixel in the TWINS ENA image

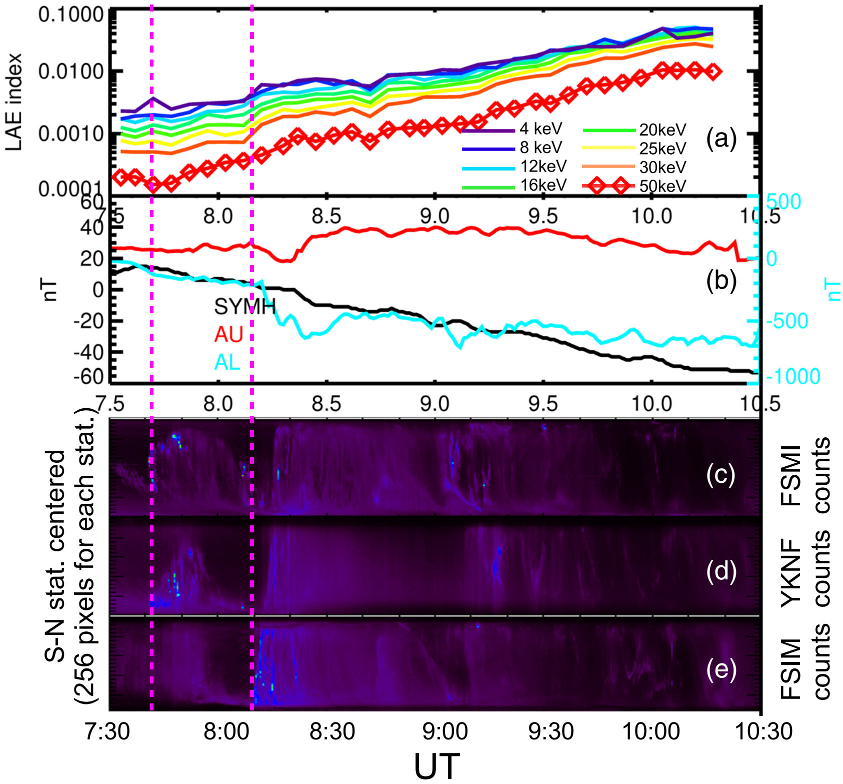

Figure 1. (a) TWINS 2 LAE index for eight energy bins; (b) geomagnetic indices SYMH, AU, and AL; and THEMIS auroral keograms from ground-based stations (c) FSMI (67.29°N, 307.05°E), (d) YKNF (69.25°N, 302.67°E), and (**e**) FSIM (67.23°N, 294.41°E) for 11 October 2008. Coordinates are geomagnetic latitude and longitude (IGRF-2010 at altitude 0 km, http://themis.igpp.ucla.edu/instrument_gmags.shtml). Note that Y scale is different for SYMH (right side of Figure 1b) and for AU/AL (left side of Figure 1b). The LAE index is defined as the intensity of the brightest pixel inside $r = 1.5\ R_E$. Two magenta lines denote a small disturbance near 0737 UT and substorm onset near 0810 UT.

inside a plane-of-sky radius of $r = 1.5R_E$. Because the ENA source is not resolved within the pixel, the maximal intensity is divided by R^2, where R is the distance from s/c to the Earth limb. The limitation $r = 1.5R_E$ is needed to exclude HAEs coming from ring current. The LAE index is calculated from TWINS 2 data with 5-min resolution. Good quality data for TWINS 2 are available for the period 0730–1020 UT. The LAE index is calculated for eight energy bins in the range 2–75 keV. To accumulate statistics, each energy bin centered at energy E is calculated with $\Delta E/E = 1$. For a detailed description of TWINS spectrometers and ENA calculations see *McComas et al.* [2009, 2012] and *Valek et al.* [2010, 2012].

[10] An example of TWINS ENA HAE images for this event can be found in *Buzulukova et al.* [2010], and the LAE for ~10 UT were analyzed in *Bazell et al.* [2010]. To identify the allowed directions for LAEs to be observed from a given spacecraft location, *Bazell et al.* [2010] introduced an emissivity function. The emissivity function is an artificial LAE emission pattern resulting from ion precipitation but with no dependence on either MLT or L. The emissivity function varies with spacecraft viewpoint. LAEs can only appear in an ENA image where the emissivity function is nonzero.

[11] For the 11 October 2008, TWINS 2 was near the apogee at $\sim 6 - 7R_E$ and spanning MLT from ~08 to ~10 h. This geometry favors observations of LAEs at 2000–2200 MLT.

[12] The THEMIS auroral keograms in Figure 1 show a small disturbance near 0737 UT. This small disturbance was localized and not manifested in AU/AL indices. Therefore, we call it "pseudo-breakup". After the pseudo-breakup, THEMIS keograms and auroral indices indicate a large substorm onset near 0810 UT.

[13] The LAE index starts to increase near 0745 UT, after the first disturbance onset. It continues to grow during substorm growth phase and intensifies after the substorm onset at 0810UT. During substorm recovery phase, the LAE index does not subside but continues to grow.

[14] Global morphology of the ion source population is analyzed with MEPED data from the NOAA18 and MetOp02 spacecrafts. Each MEPED telescope has two sets of detectors, with one pointed to the Earth to measure particles near the loss cone (meped0 channel) with a 30° field of view, and the second pointed transverse to the satellite track to measure locally mirroring particles (meped90 channel) with a 30° field of view at ~800 km altitude. Further information about MEPED telescopes can be found in *Sørbø et al.* [2009] and references therein.

[15] MEPED data for this case are shown in Figure 2, with meped0 and meped90 channels before the beginning of the disturbance (top panel), near the substorm onset (middle panel), and 1 h after the substorm onset, near SYMH minimum. The time interval 0730–1030 UT corresponds to storm main phase. We identify strong fluxes at low latitudes (~60°) with ring current fluxes. Because both meped0 and meped90 channels show similar fluxes at low latitudes for all time intervals, we conclude that the pitch angle distribution function of the ring current remains close to isotropic (at least at ~800 km altitude). We also observe that LAEs continue to grow during the storm main phase together with the SYMH index. We conclude the intense LAEs were produced by ring current particles continuously filling the loss cone during the storm main phase. It should be noted that some NOAA/MetOp measurements were taken in the

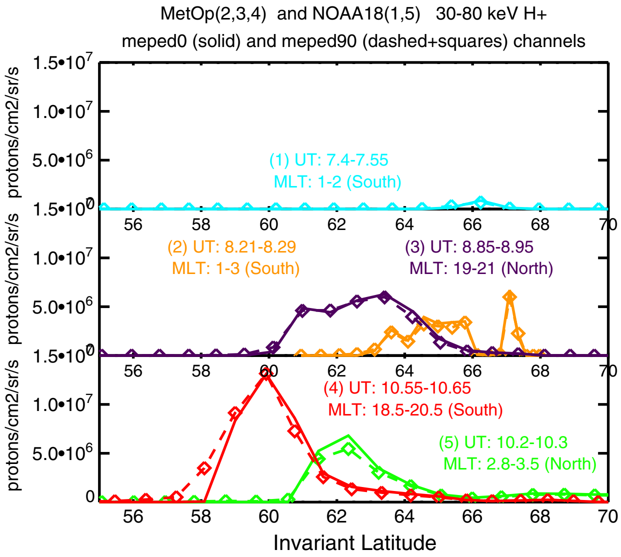

Figure 2. NOAA and MetOp MEPED measurements of proton fluxes for 11 October 2008 in the energy range 30–80 keV versus invariant latitude before substorm onset (top panel), near substorm onset (middle panel), and 1 h after substorm onset (bottom panel). Solid lines show meped0 channel measuring loss cone particles with 30° field of view. Dashed lines with symbols show meped90 channel measuring locally trapped particles with 30° field of view. Similar flux level for both channels indicates a high level of isotropy.

Southern Hemisphere while TWINS 2 was in the Northern Hemisphere. We assume that the ring current and most of LAEs are formed on closed field lines and should be similar in the two hemispheres. A good correspondence between TWINS 2 LAEs and DMSP particle data from the opposite hemisphere were also obtained in *Bazell et al.* [2010].

[16] Figure 3 shows an ionospheric projection of the regions where NOAA/MetOp measurements were sampled. For regions 1, 2, and 4 from the Southern Hemisphere, we reversed a sign of the invariant latitude. The gray crescent represents a sketch of the TWINS 2 emissivity function taken from *Bazell et al.* [2010]. The color code and numbering for NOAA/MetOp satellites are the same as for the Figure 2. Since the TWINS 2 emissivity function covers regions 3 and 4 only, NOAA/MetOp observations from regions 1, 2, and 5 help to provide the global picture of ion distribution.

3. 5 April 2010 Event

[17] Figure 4 displays the LAE index (panel a), AU/AL/SYMH indices (panel b), and THEMIS all-sky imager observations for seven stations for the 5 April 2010 event, 0800–1100 UT (panels c–i). The LAE index is calculated from TWINS 1 data with 5-min resolution for 0835–0935 UT. Data before 0835 UT and after 0935 UT are not shown due to background contamination. TWINS 1 was near apogee at $\sim 7R_E$ and with MLT from ~0930 h (around 0830 UT) to ~1030 h (around 0930 UT). This geometry is favorable for observations of LAEs at 2130–2230 h. An example of TWINS ENA images with both ring current emissions and LAEs can be found in *McComas et al.* [2012]. The TWINS 1 viewing geometry for the 5 April 2010 event was approximately the

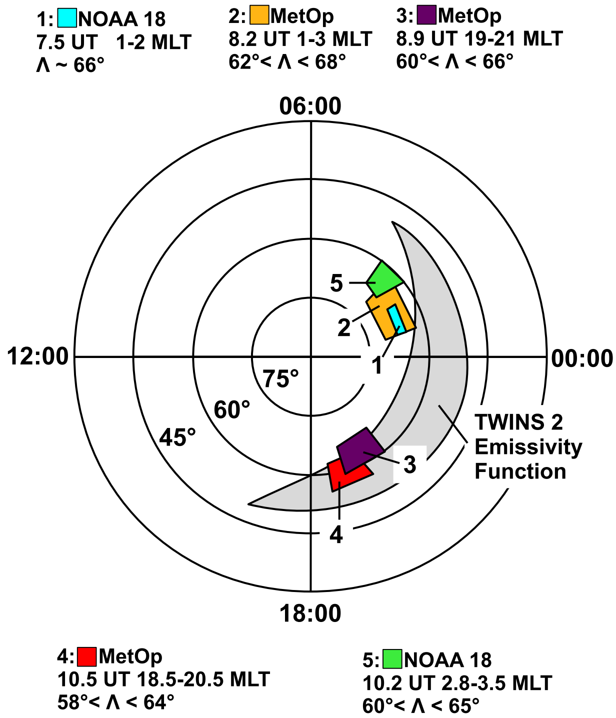

Figure 3. Schematic of the NOAA/MetOp ion measurements for 11 October 2008 shown in Figure 2. Color code and numbering for spacecraft are the same as for Figure 2. The gray crescent is a sketch of the TWINS 2 emissivity function taken from *Bazell et al.* [2010] that delineates where LAEs can be observed at the spacecraft location.

same as for the TWINS 2 for the 11 October 2008 event, justifying direct comparison of LAEs for two cases.

[18] A large substorm occurred at 0903 UT and produced extremely disturbed geomagnetic conditions [*Connors et al.*, 2011]. Small disturbances started before substorm onset, around 0847 UT, and were manifested as small dipolarization at GOES 11 reported in *Connors et al.* [2011]. The LAE index starts to grow near 0847 UT for all energy bins, well before substorm onset but around the same time as GOES observed a small dipolarization. This dipolarization was not accompanied by magnetic field signatures of a substorm at ~11 R_E [*Connors et al.*, 2011]. For high energies, the LAE index peaked around 09 UT, at substorm onset, and then subsided. For low energies, the peak of the LAE index tends to arrive later in time, after the substorm onset. The lower energy bin at 4 keV (2–6 keV) does not show a significant decrease after the onset.

[19] Global morphology of source ion population is analyzed with MEPED data from the NOAA16, NOAA19, and MetOp02 spacecrafts. Figure 5 shows MEPED 30–80 keV H^+ fluxes for 5 April 2010. The top panel of the figure shows MetOp02 data before the disturbance occurs. Proton fluxes are small, and there is no significant difference between the meped0 and meped90 channels. This indicates a high level of isotropy near the loss cone. The middle plot shows NOAA19 and MetOp data near the substorm onset when the LAE index for this energy range has a maximum. Both trapped and loss cone fluxes increase. At dusk, the isotropic boundary [*Sergeev et al.*, 1993] appears at 61.5° invariant latitude. This indicates the formation of a trapped population at low latitudes. The difference becomes dramatic at ~0930 UT (bottom panel of Figure 5) when the LAE index subsides.

[20] During 0930–1015 UT, the SYMH index continues to diminish, indicating storm main phase, and reaches minimum near 1045 UT. We therefore identify a trapped population at low latitudes with the ring current. Low fluxes in the meped0 channel indicate an almost empty loss cone for ring current ions. Since LAEs are formed below 800 km [*Roelof*, 1997; *Bazell et al.*, 2010], the ring current at low latitudes produces the low LAE flux. We stress that MEPED telescopes have a 30° field of view. The meped0 channel can measure a mixed population of loss cone/trapped particles [*Sørbø et al.*, 2009]. Very low fluxes for the meped0 channel therefore indicate that not only is the loss cone empty but also that there are no particles near the loss cone.

[21] Figure 6 shows the ionospheric projection of the regions where NOAA/MetOp measurements were sampled. For the regions from the Southern Hemisphere, we reversed the sign of the invariant latitude. The gray crescent represents a sketch of the TWINS 1 emissivity function. Because the viewing geometry was similar for the 11 October 2008 and 5 April 2010 events, we assume that the emissivity function was similar for both cases. The color code and numbering for NOAA/MetOp satellites are the same as for the Figure 5. As for the previous case of 11 October 2008, the NOAA/MetOp observations help to provide a global picture of ion distribution. LAEs from regions 3, 4, and 6 were directly observed by TWINS 1.

4. Discussion

[22] We find that the LAE responses to substorms were very different for the two cases. For 11 October 2008, LAEs start to grow after pseudo-breakup near 0745 UT, continue to grow during substorm growth phase, intensify after substorm onset near 0810 UT, and continue to grow even during substorm recovery phase. For 5 April 2010, the LAE index peaks at substorm onset and subsides during recovery phase after the auroral expansion (except 2- to 6-keV energy bins). It is tempting to think that for both cases the LAE index might serve as a precursor of substorm activity. However, for the 11 October event, the LAE intensification correlates with the onset of pseudo-breakup near 0745 UT. The transition between pseudo-breakup and small substorm is probably smooth (e.g., *Rostoker* [1998] and *Kullen et al.* [2010]), so one may argue that the LAE onset corresponds to the onset of a very small substorm. Therefore, one interpretation is that the LAE intensification marks the onset of activity in the magnetotail leading to expansion of the large substorm with AE ~ 500 nT.

[23] For 5 April 2010, the LAE onset coincides with a small dipolarization at $L = 6.6$ at 0845 UT. It is natural to explain it with the onset of geomagnetic activity bringing particles closer to the Earth and causing the LAE intensification. This process ended with the onset of a large substorm (AE > 1000 nT) near 0902 UT. Therefore, for both cases, the LAE intensification marks the initiation of processes in the magnetotail that bring particles closer to the Earth causing the LAE intensification.

[24] It is known that an interval of southward interplanetary magnetic field (IMF) Bz component is normally required for the substorm growth phase [*McPherron*, 1972; *Lyons et al.*,

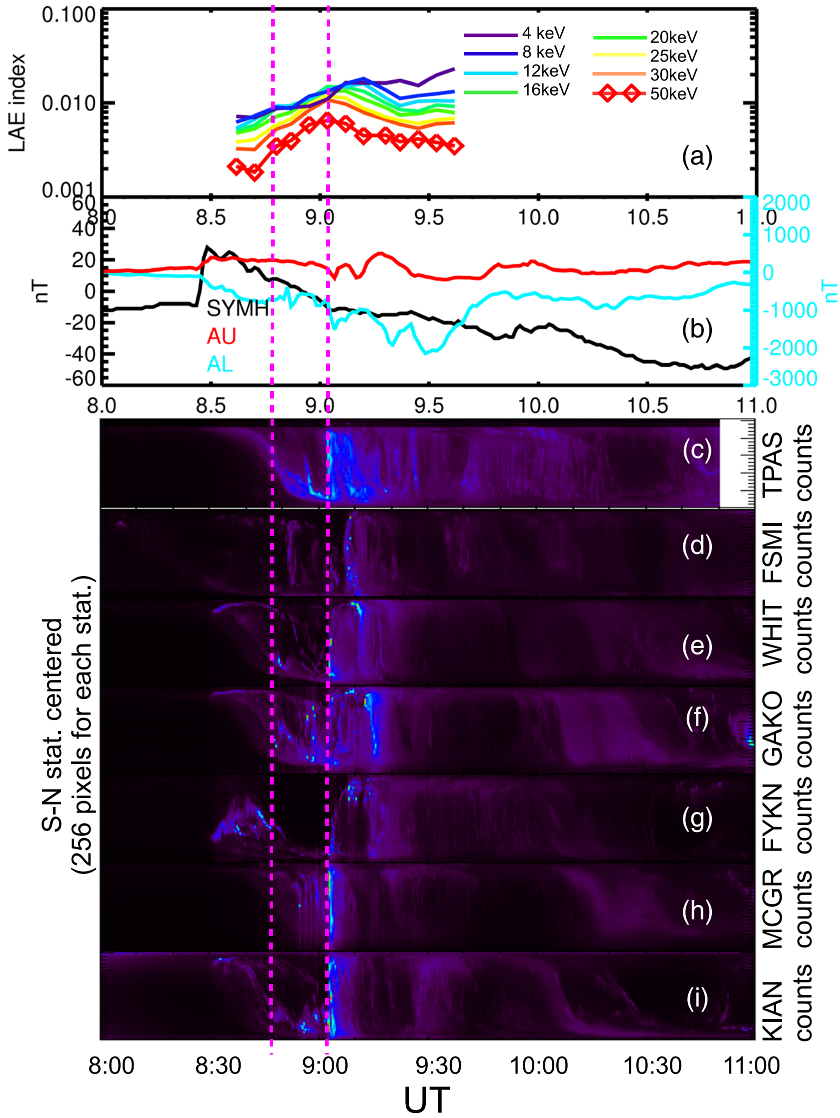

Figure 4. (a) TWINS 1 LAE index for eight energy bins, (b) geomagnetic indices, and THEMIS auroral keograms for seven ground-based stations (**c**) TPAS (63.12°N, 324.23°E), (d) FSMI (67.29°N, 307.05°E), (e) WHIT (63.64°N, 279.62°E), (**f**) GAKO (63.05°N, 269.51°E), (g) FYKN (67.25°N, 266.67°E), (h) MCGR (61.74°N, 260.25°E), and (**i**) KIAN (65.00°N, 251.50°E) for 5 April 2010. Coordinates are geomagnetic latitude and longitude (IGRF-2010 at altitude 0 km, http://themis.igpp.ucla.edu/instrument_gmags.shtml). Two magenta lines denote dipolarization ($L = 6.6$) near 0847 UT and onset of a large substorm near 0903 UT.

1997; *Morley and Freeman*, 2007]. One possible mechanism for the intensification of LAEs is enhanced convection during the substorm growth phase which brings particles closer to the Earth and causes intensification of particle fluxes. The other mechanism may be related to the earthward motion of the proton isotropy boundary during the substorm growth phase [*Sergeev et al.*, 1990]. Both mechanisms produce equatorward motion of pre-onset arcs (e.g., *Mende et al.* [2003]).

[25] Recently, *Gilson et al.* [2012] employed the OpenGGCM MHD code to model proton and electron precipitation during a substorm. For electrons, they calculated "diffuse" precipitation from MHD fluxes; for ions, they multiplied the MHD-calculated precipitation by factor f, where $f = 0$ equatorward of the ion isotropy boundary and $f = 1$ poleward of the isotropy boundary. $f = 1$ if $0 < \leq \kappa \leq \sqrt{8}$ where κ parameter [*Buechner and Zelenyi*, 1987] is calculated from equatorial MHD temperature and magnetic field radius of curvature.

[26] In this interpretation, the isotropy boundary is defined by intense scattering of protons into the loss cone due to high curvature of the geomagnetic field in the equatorial plane [*Sergeev et al.*, 1990]. Equatorward motion occurs for both ion and electron pre-onset arcs [*Gilson et al.*, 2012, Figure 1]. These results favor enhanced convection as a reason for pre-onset intensification of proton arcs, and thus of LAEs. It is interesting that the proton precipitation from *Gilson et al.* [2012, Figure 1] resembles the dynamics of LAEs for the 5 April 2010 event, i.e., the intensity peaks around the time of substorm onset. *Gilson et al.* [2012] also noted that substorm dipolarization should, in general, diminish proton precipitation because enhanced Bz should

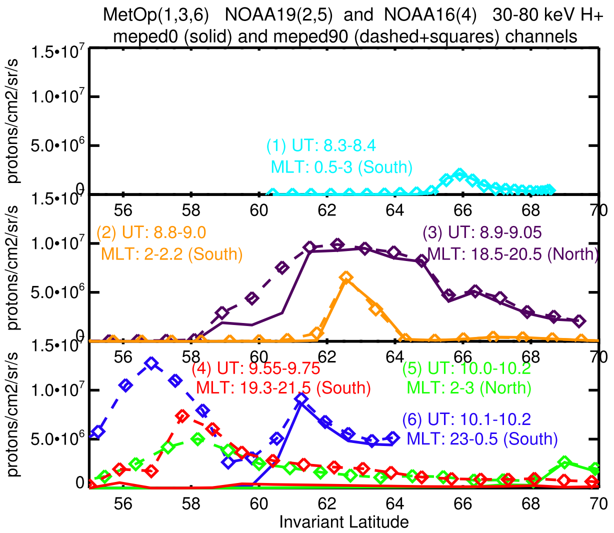

Figure 5. NOAA and MetOp MEPED measurements of proton fluxes for 5 April 2010 in the energy range 30–80 keV versus invariant latitude before substorm onset (top panel), near substorm onset (middle panel), and 1 h after substorm onset (bottom panel). The format is the same as for Figure 2.

reduce or cease scattering into the loss cone. These published results suggest that for the 5 April 2010 event, the existence of the isotropy boundary in the inner magnetosphere limited ion precipitation during the substorm expansion phase when substorm depolarizaion was in progress.

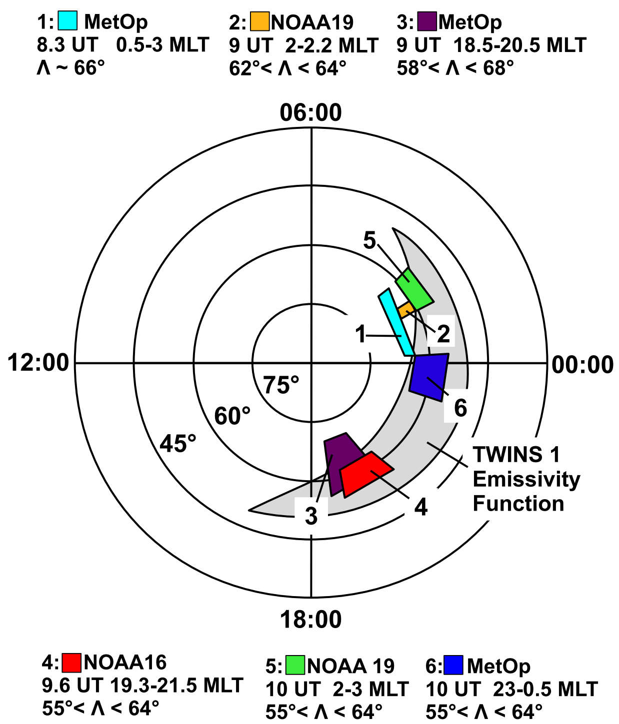

Figure 6. Schematic of the NOAA/MetOp ion measurements for 5 April 2010 shown in Figure 5. Color code and numbering for spacecraft are the same as for Figure 5. The gray crescent is a sketch of the TWINS 1 emissivity function. We assume here that the emissivity function is the same as for 11 October 2008.

[27] According to *Gilson et al.* [2012], several main factors that control the flux of precipitating protons at a given ionospheric location are equatorial plasma temperature (particle gyroradius), magnitude of the equatorial magnetic field, and the flux intensity. These factors control the scattering of protons into the loss cone due to magnetic field line curvature, and hence should control LAE production. Other non-MHD processes, especially during substorm expansion phase, may operate, but their role is still unclear.

[28] In the inner magnetosphere, the scattering due to magnetic field line curvature does not operate under normal conditions because of large equatorial Bz magnitude and small curvature of more dipole-like fields. It is surprising that for the isotropy boundary to play a role in the LAE dynamics of the CIR-driven storm of 11 October 2008, the isotropy boundary must be located deep inside the inner magnetosphere, suggesting that other mechanisms are responsible for the scattering of protons into the loss cone. For CIR storms, fluctuations in IMF Bz component may cause numerous small injections and fluctuations in the location of the isotropy boundary for protons [*Sørbø et al.*, 2009]. This activity may intensify wave-particle interactions and cause isotropization of the distribution function in the inner magnetosphere for the 11 October 2008 event. However, it is difficult to make general conclusions here based on the analysis of one CIR event and one CME event.

[29] After the substorm onset, the LAE dynamics were different for the two cases. Based on NOAA/MetOp observations, we suggest the following explanation. The 11 October 2008 event was a substorm that occurred during the main phase of a CIR storm. The loss cone was filled with protons from the ring current. Both trapped and loss cone fluxes continued to grow during the recovery phase of the substorm and the main phase of the storm. The LAE index in this case followed roughly the SYMH index.

[30] For 5 April 2010, substorm activity was considerably larger than that of the 11 October 2008 event. Strong substorm precipitations removed all particles near the loss cone, leaving only a trapped population. Near SYMH minimum at ~10 UT, the ring current (30–80 keV) was represented by a trapped population. There were no particles inside or near the loss cone. At the same time, the LAE index subsided. This result is consistent with the LAE theory [*Roelof*, 1997; *Bazell et al.*, 2010] where the LAE production is confined to a nearly mirroring population within a narrow altitude range of ~200–300 km.

[31] Although auroral activity was different for the 5 April and the 11 October substorms, the Dst response was similar with ~−50 nT from 10 to 12 UT. We suggest that for the 5 April event, strong substorm activity caused intense (proton and electron) precipitation, emptying the flux tube content and diminishing the "seed" population for the ring current at high geomagnetic latitudes. We also note that the ring current characteristics were different for the same value of the Dst index (~ − 50 nT) near 10 UT (for both events). First, NOAA data display different pitch angle distributions (at least at ~800 km) for underlying ring current population. Second, the ring current appears at lower latitudes for the 5 April 2010 event, indicating stronger injection effects. These differences may also be related to the storm type, e.g., CME event (5 April 2010) versus CIR event (11 October 2008).

[32] A statistical study of proton substorm aurora was carried out by *Mende et al.* [2003]. From an analysis of ~100 substorms observed by the IMAGE/FUV instrument, they conclude that proton substorm aurora follow the same dynamics as electron aurora. They both occur at the same MLT and sharply increase at substorm onset. The proton aurora subsides to pre-onset level during the first 30–60 min of the recovery phase. We compare here the dynamics of substorm proton aurora with dynamics of LAEs for the two substorms considered. For 11 October 2008, the LAE index grows together with the SYMH index and does not follow substorm phases. For 5 April 2010, the LAE index starts to grow before the large substorm onset and has energy dependence. Therefore, the LAE dynamics are different from the dynamics of proton aurora (at least as described by *Mende et al.* [2003]).

[33] It is important to understand why the LAE time histories for the 5 April 2010 event are different for different energies. This feature is also noted in *McComas et al.* [2012] although the LAE index has been calculated in a different way. Around 0900 UT, the brightest fluxes for 8- and 50-keV energy bins come from different pixels of the sky. This means that the spatial structure of LAEs is different for different energies as was pointed out by *Bazell et al.* [2010] for the 11 October event. We can interpret the timing profile for the LAE index as the result of increased plasma transport into the inner magnetosphere under enhanced convection/substorm injection. Energy-dependent processes of loss cone filling and motion of source ion structures during different substorm phases may account for energy dispersion in the LAE index. For example, scattering on field line curvature depends on particle energy, wave-particle interactions may be energy-dependent, and motion of source ion structures in the inner magnetosphere depends on kinetic energy via the balance of ExB drift and the gradient and curvature drift.

[34] It is reasonable to suggest that the LAE intensification starts in the same region where pre-onset proton arcs are found, i.e., at the same region where pre-onset precipitating protons are observed [*Mende et al.*, 2003; *Milan et al.*, 2009]. This conclusion is consistent with the findings of *Bazell et al.*, [2010] where they show that the LAE production for the 11 October 2008 event maps into the diffuse ion precipitation region as seen by the DMSP spacecrafts. This region maps close to the inner edge of the plasma sheet, to the transition zone between the tail and the inner magnetosphere. According to several recent substorm studies, this is the same place where substorm onset occurs [*Sergeev et al.*, 2012a, 2012b]. We believe that a careful analysis (both experimental and modeling) of LAE dynamics may shed light on the role of energetic particles of outer ring current/radiation belts in substorm dynamics.

[35] Our analysis also suggests that the LAE production may move/expand into the inner magnetosphere and blend with the ring current emissions when the ring current is formed. The motion/expansion is modulated by the pitch angle distribution of the ring current and may be energy dependent.

5. Conclusions

[36] Based on the analysis of TWINS 1 and 2 LAEs and NOAA/MetOp measurements of proton fluxes at 30–80 keV, we conclude the following:

[37] 1. The timing and intensity profiles of LAEs are different for the two events. For a substorm occurring during the main phase of a CIR storm (11 October 2008), LAEs seem roughly correlated with the SYMH index and continue to grow during the storm main phase. For a substorm occurring during the main phase of a CME storm (5 April 2010), LAEs do not follow the SYMH index but rather follow roughly the auroral activity and peak near substorm onset.

[38] 2. Different LAE behavior results from different pitch angle distributions of the two source ion populations. On 11 October 2008, the trapped and loss cone populations at ~800 km altitude were approximately the same. This indicates formation of a ring current with a distribution function close to isotropic near the loss cone. LAE dynamics are coupled with ring current dynamics during the event. On 5 April 2010, intense precipitation occurred during a large substorm. During substorm recovery, the loss cone for the ring current population is almost empty. The LAE production subsides, and LAEs become decoupled from the SYMH index and from the ring current. This result is consistent with the LAE theory predicting that the LAE production is confined to a narrow altitude range near ~200–300 km and is produced by nearly mirroring ions.

[39] 3. Our results are consistent with the LAE production starting in the transition region between the magnetotail and inner magnetosphere before a substorm onset. After the substorm onset, LAEs may expand/move into the inner magnetosphere together with the formation of the ring current and blend with ENA emissions from the ring current. This expansion/motion is modulated by a pitch angle distribution of the ring current population and may be energy dependent.

[40] 4. LAE measurements of substorms by TWINS are limited by the specific viewing geometry. Despite these limitations, the method offers a unique opportunity to study a substorm-related global picture of particle transport and energization.

[41] **Acknowledgments.** We acknowledge THEMIS data provider, S. Mende and E. Donavan at UCB and University of Calgary, respectively, NASA NASS-0289 and CDAWeb. SYMH, AU, and AL data were obtained from Kyoto WDC for Geomagnetism. NOAA/MetOp data were obtained from the NOAA website http://www.ngdc.noaa.gov/stp/satellite/poes/dataaccess.html. Coordinates of the THEMIS stations were taken from the THEMIS website http://themis.igpp.ucla.edu/instrument_gmags.shtml. This work was carried out as a part of the TWINS mission, which is part of NASA's Explorer Program. The effort at JHU/APL was carried out under subcontract 799106L from SWRI. For N.B. and M.-C.F., this work was also supported by NASA Heliophysics Guest Investigators Program, under Work Breakdown Structure 955518.02.01.02.57.

References

Bazell, D., E. C. Roelof, T. Sotirelis, P. C. Brandt, H. Nair, P. Valek, J. Goldstein, and D. McComas (2010), Comparison of TWINS images of low-altitude emission of energetic neutral atoms with DMSP precipitating ion fluxes, *J. Geophys. Res. (Space Physics)*, *115*, A10,204, doi:10.1029/2010JA015644.

Brandt, P. C., S. Barabash, O. Norberg, R. Lundin, E. C. Roelof, C. J. Chase, B. H. Mauk, and M. Thomsen (1997), ENA imaging from the Swedish micro satellite Astrid during the magnetic storm of 8 February, 1995, *Adv. Space Res.*, *20*, 1061–1066.

Buechner, J., and L. M. Zelenyi (1987), Chaotization of the electron motion as the cause of an internal magnetotail instability and substorm onset, *J. Geophys. Res.*,*92*, 13,456–13,466, doi:10.1029/JA092iA12p13456.

Buzulukova, N., M.-C. Fok, J. Goldstein, P. Valek, D. J. McComas, and P. C. Brandt (2010), Ring current dynamics in moderate and strong storms: Comparative analysis of TWINS and IMAGE/HENA data with the Comprehensive Ring Current Model, *J. Geophys. Res. (Space Physics)*, *115*, A12,234, doi:10.1029/2010JA015292.

Connors, M., C. T. Russell, and V. Angelopoulos (2011), Magnetic flux transfer in the 5 April 2010 Galaxy 15 substorm: An unprecedented observation, *Ann. Geophys.*, *29*, 619–622, doi:10.5194/angeo-29-619-2011.

Gilson, M. L., J. Raeder, E. Donovan, Y. S. Ge, and L. Kepko (2012), Global simulation of proton precipitation due to field line curvature during substorms, *J. Geophys. Res. (Space Physics)*, *117*, A05216, doi:10.1029/2012JA017562.

Kullen, A., T. Karlsson, J. A. Cumnock, and T. Sundberg (2010), Occurrence and properties of substorms associated with pseudobreakups, *J. Geophys. Res. (Space Physics)*, *115*, A12310, doi:10.1029/2010JA015866.

Lyons, L. R., G. T. Blanchard, J. C. Samson, R. P. Lepping, T. Yamamoto, and T. Moretto (1997), Coordinated observations demonstrating external substorm triggering, *J. Geophys. Res.*, *102*, 27,039–27,052, doi:10.1029/97JA02639.

McComas, D. J., et al. (2009), The Two Wide-angle Imaging Neutral-atom Spectrometers (TWINS) NASA Mission-of-Opportunity, *Sp. Sci. Rev.*, *142*, 157–231, doi:10.1007/s11214-008-9467-4.

McComas, D. J., N. Buzulukova, M. G. Connors, M. A. Dayeh, J. Goldstein, H. O. Funsten, S. Fuselier, N. A. Schwadron, and P. Valek (2012), Two Wide-Angle Imaging Neutral-Atom Spectrometers and Interstellar Boundary Explorer energetic neutral atom imaging of the 5 April 2010 substorm, *J. Geophys. Res. (Space Physics)*, *117*, A03225, doi:10.1029/2011JA017273.

McPherron, R. L. (1972), Substorm related changes in the geomagnetic tail: The growth phase, *Planet. Space Sci.*, *20*, 1521, doi:10.1016/0032-0633(72)90054-2.

Mende, S. B., H. U. Frey, T. J. Immel, D. G. Mitchell, P. C. son-Brandt, and J.-C. Gérard (2002), Global comparison of magnetospheric ion fluxes and auroral precipitation during a substorm, *Geophys. Res. Lett.*, *29*(12), 1609, doi:10.1029/2001GL014143.

Mende, S. B., H. U. Frey, B. J. Morsony, and T. J. Immel (2003), Statistical behavior of proton and electron auroras during substorms, *J. Geophys. Res. (Space Physics)*, *108*, 1339, doi:10.1029/2002JA009751.

Mende, S. B., S. E. Harris, H. U. Frey, V. Angelopoulos, C. T. Russell, E. Donovan, B. Jackel, M. Greffen, and L. M. Peticolas (2008), The THEMIS array of ground-based observatories for the study of auroral substorms, *Space Sci. Rev.*, *141*, 357–387, doi:10.1007/s11214-008-9380-x.

Milan, S. E., A. Grocott, C. Forsyth, S. M. Imber, P. D. Boakes, and B. Hubert (2009), A superposed epoch analysis of auroral evolution during substorm growth, onset and recovery: Open magnetic flux control of substorm - intensity, *Ann. Geophys.*, *27*, 659–668, doi:10.5194/angeo-27-659-2009.

Morley, S. K., and M. P. Freeman (2007), On the association between northward turnings of the interplanetary magnetic field and substorm onsets, *Geophys. Res. Lett.*, *34*, L08104, doi:10.1029/2006GL028891.

Pollock, C. J., et al. (2003), The Role and Contributions of Energetic Neutral Atom (ENA) imaging in magnetospheric substorm research, *Sp. Sci. Rev.*, *109*, 155–182, doi:10.1023/B:SPAC.0000007518.93331.d5.

Pollock, C. J., A. Isaksson, J.-M. Jahn, F. Søraas, and M. Sørbø (2009), Remote global-scale observations of intense low-altitude ENA emissions during the Halloween geomagnetic storm of 2003, *Geophys. Res. Lett.*, *36*, L19,101, doi:10.1029/2009GL038853.

Roelof, E. C. (1997), ENA emission from nearly-mirroring magnetospheric ions interacting with the exosphere, *Adv. Space Res.*, *20*, 361–366, doi:10.1016/S0273-1177(97)00692-3.

Rostoker, G. (1998), On the place of the pseudo-breakup in a magnetospheric substorm, *Geophys. Res. Lett.*, *25*, 217–220, doi:10.1029/97GL03583.

Sergeev, V., Y. Nishimura, M. Kubyshkina, V. Angelopoulos, R. Nakamura, and H. Singer (2012a), Magnetospheric location of the equatorward prebreakup arc, *J. Geophys. Res. (Space Physics)*, *117*, A01212, doi:10.1029/2011JA017154.

Sergeev, V. A., P. Tanskanen, K. Mursula, A. Korth, and R. C. Elphic (1990), Current sheet thickness in the near-earth plasma sheet during substorm growth phase, *J. Geophys. Res. (Space Physics)*, *95*, 3819–3828, doi:10.1029/JA095iA04p03819.

Sergeev, V. A., M. Malkov, and K. Mursula (1993), Testing the isotropic boundary algorithm method to evaluate the magnetic field configuration in the tail, *J. Geophys. Res. (Space Physics)*, *98*, 7609–7620, doi:10.1029/92JA02587.

Sergeev, V. A., V. Angelopoulos, and R. Nakamura (2012b), Recent advances in understanding substorm dynamics, *Geophys. Res. Lett.*, *39*, L05101, doi:10.1029/2012GL050859.

Sørbø, M., F. Søraas, M. I. Sandanger, and D. S. Evans (2009), Ring current behaviour during corotating interaction region and high speed stream events, *JASTP*, *71*, 1103–1125, doi:10.1016/j.jastp.2008.08.012.

Valek, P., P. C. Brandt, N. Buzulukova, M.-C. Fok, J. Goldstein, D. J. McComas, J. D. Perez, E. Roelof, and R. Skoug (2010), Evolution of low-altitude and ring current ENA emissions from a moderate magnetospheric storm: Continuous and simultaneous TWINS observations, *J. Geophys. Res. (Space Physics)*, *115*, A11, 209, doi:10.1029/2010JA015429.